AIAA JOURNAL
Vol. 43, No. 10, October 2005

Skin-Friction Reduction on Body of Revolution Using Boundary-Layer Alteration Devices

Vladimir I. Kornilov*
Russian Academy of Sciences, 630090, Novosibirsk, Russia

The effect of boundary-layer alteration devices (BLADEs) on the characteristics of a turbulent boundary layer on an axisymmetric body of revolution in nominally zero pressure gradient incompressible flow is experimentally studied. The Reynolds numbers based on momentum thickness at the BLADEs' position were varied from 2610 to 6500. All BLADE configurations that were examined, including single-element ones, are shown to be capable of reducing skin friction in the downstream region. A tandem BLADE configuration is found to be more advantageous than the single-element configuration. The tandem configuration, formed by two flat ring elements with a chord length within 75% of the boundary-layer thickness, reduces the net drag by at least 15% compared to the regular flow. An enhanced drag reduction is also observed for small positive angles of attack of the BLADE. Finally it is found that an increase in the chord length of ring elements degrades the BLADE's effectiveness.

Nomenclature

C_f	=	local skin-friction coefficient
C_P	=	static-pressure coefficient, $(P - P_\infty)/q_\infty$
E_t	=	nondimensionalized thickness of the excess kinetic energy; Eq. (4)
G	=	Clauser nonequilibrium parameter; Eq. (3)
H	=	boundary-layer shape factor, δ^*/θ
h	=	wall-normal position of ring element in the boundary layer
L	=	overall length of body of revolution
l	=	ring-element chord length
P_∞	=	reference static pressure
q	=	dynamic pressure, $\rho U^2/2$
R	=	lateral radius of curvature
Re_L	=	reference Reynolds number, UL/ν
s	=	streamwise spacing between tandem ring elements
U_∞	=	reference freestream velocity
u'	=	streamwise velocity fluctuation
v_*	=	dynamic velocity, $\sqrt{(\tau_w/\rho)}$
x	=	streamwise coordinate
y	=	crosswise coordinate, distance from wall
α	=	ring-element angle of attack
ΔC_F	=	net drag reduction coefficient; Eq. (5)
Δx	=	downstream distance from the ring-element trailing edge
δ	=	boundary-layer 99% thickness
δ^*	=	boundary-layer displacement thickness
θ	=	boundary-layer momentum thickness
ν	=	kinematic viscosity
ρ	=	density
τ	=	shear stress

Subscripts

e	=	boundary-layer edge conditions
L	=	based on the body length
w	=	wall conditions
0	=	BLADE location conditions or total pressure
1, 2	=	first or second ring element
∞	=	freestream conditions

Superscript

$(^-)$	=	time-averaged value

Received 26 January 2005; revision received 16 May 2005; accepted for publication 16 May 2005.

*Assistant Professor and Leading Scientist, Department of Experimental Aerogasdynamics, Institute of Theoretical and Applied Mechanics, Siberian Branch.

I. Introduction

THE topic of energy conservation, which has been of considerable interest over the past two or three decades, is a motivation for studies aimed at aircraft drag reduction. Undoubtedly, aircraft drag reduction will remain a challenging topic in the future, too. It is known that the skin-friction drag of long-range airliners is a substantial portion of the total drag: at cruise this contribution amounts to 50%. For submarines and torpedoes, the skin-friction contribution is 65–70% of the total drag. Thus, skin-friction reduction offers tremendous potential in energy savings.

There are two approaches to skin-friction drag reduction. The first, traditional approach is aimed at improving the aerodynamic shape and surface finish. Within this approach, most of the methods for drag reduction have been exhausted. The second approach is the application of artificial management methods to affect the structure of the near-wall turbulence.

Starting from the mid-1970s, researchers have gained considerable insight into turbulent skin-friction reduction by various passive and/or active control methods in turbulent shear flows.[1–5] The hierarchy of these methods is shown pictorially in Ref. 6. It is shown that active methods based on reactive and feedback control, or advanced adaptive systems, have in recent years been the primary focus. Nonetheless, passive control methods are still of significance and remain in use because drag reduction can be achieved with no energy input. In addition, the typical operating costs of passive control methods are much lower than those of active control methods.

This paper reports the results of an experimental investigation of the effect of eddy breakup devices on the characteristics of a turbulent boundary layer over an axisymmetric body of revolution. The eddy breakup devices are employed to reduce the skin friction. Previous studies show that the mechanisms underlying the drag reduction are more diversified and complex than simply the breakup of large eddies. For this reason, we use the term boundary-layer alteration devices (BLADEs) to describe these control effectors.

The use of passive devices called BLADEs to reduce skin friction in turbulent shear flow is not new. The basic approach of such devices is to suspend horizontal, streamwise-oriented, thin ribbons (or other elements) within the turbulent boundary layer. The objective is to use these devices to break up the large vortical (coherent) structures that are of comparable scale to the boundary-layer thickness.

The reduction of the characteristic turbulence length scale by such devices modifies the mechanism of mass transfer between different layers of fluid, thus reducing the skin friction.

In the overwhelming majority of previous studies,[7–15] the effectiveness of the BLADE was examined in two-dimensional, flat-plate, boundary layers and the BLADEs consisted of one or two (tandem configuration) elements. In some cases, the devices are found to be effective in reducing the friction drag by 10–30% (Refs. 8, 11, and 15). As for the net drag reduction, this very seldom exceeds 7–8% (Refs. 7 and 8). The experiments performed at NASA Langley Research Center have been more successful in skin-friction reduction, with a net drag reduction of up to 10%. These results are reported by Hefner.[2] However, in some cases, notably that of Sahlin et al.,[9] a net drag reduction was obtained of no more than 2% because of the high device drag. Bertelrud et al.[10] observed that the net drag reduction is dependent on both device drag and device geometry. Whereas fuselagelike bodies are of much practical interest, to the author's knowledge, this configuration was studied only in Ref. 16. Unlike wing surfaces, on which an extended region of laminar flow normally arises and for which a broad range of control is available, the boundary layer on bodies of revolution is turbulent almost from the very beginning of its development; this boundary layer is, therefore, hard to manipulate.

Unlike the papers just cited, the primary focus in the present study is the effect of flow parameters and geometric characteristics of BLADEs on the effectiveness BLADEs installed on a body of revolution. The need for such studies is obvious. It is known[4] that the classical list of relevant parameters for such devices includes a number of geometrical parameters such as the BLADE chord length l, the wall-normal position h of BLADE in the boundary layer, the BLADE's thickness t, the streamwise spacing s between the two ring elements in the tandem configuration, the gap g between the ring elements, and the boundary-layer thickness δ_0 at the position of the upstream BLADE element. An analysis shows that, even for the case of a flat plate, the majority of reported data on BLADE optimization are obtained for different experimental conditions; for this reason, these data lack a systematic character and consistency. Possibly for this reason, no attempts have been made to generalize the available data set. For instance, in several works[12,13] the optimum BLADE chord length l is recommended to be the same order as the boundary-layer thickness δ_0. A decrease in the ratio l/δ_0 is reported to have a smaller influence on the drag reduction than the wall-normal position of the BLADE. In this regard, in the present study, we focus on the effect of h on the effectiveness of the BLADE. On the whole, we confirm that the wall-normal position of the BLADE is of significance. However, it is found that the previously reported (e.g., Ref. 11) optimum ratio, l/δ_0, is not applicable to bodies of revolution; in fact the effect of the BLADE chord length is also pronounced. As for the streamwise spacing s between two elements in the tandem configuration, the majority of previous authors find that a spacing s of order $(10–12)\delta_0$ is optimum. Preliminary experiments[17,18] on a body of revolution confirm this finding, and thus, it is possible to compile a list of the geometric parameters that determine the effectiveness of BLADEs.

II. Experimental Conditions and Procedure

The tests were carried out in the closed-return subsonic low-turbulence wind tunnel at freestream flow velocities $U_\infty = 8$, 15, 25, and 32 m/s, yielding Reynolds numbers, based on the length L of the model, $Re_L = 1.44 \times 10^6$, 2.61×10^6, 4.35×10^6, and 5.54×10^6.

The experiments were performed on a body of revolution of length $L = 2600$ mm (Fig. 1). This model is sting mounted in the test section of the wind tunnel on a rigid pylon. The model consists of a leading part, which is an ellipsoid of revolution, whose major semi-axis was 300 mm, and a cylindrical part that is 100 mm in diameter. To avoid problems with model bending and to suppress vibrations that could emerge in the flow, the model is provided with an additional streamlined support. The boundary layer on the model is artificially tripped. This is done using a boundary-layer tripping ring made from a wire that is 1.6 mm in diameter and positioned 300 mm downstream of the nose of the body. There are 22 static pressure orifices 0.4 mm in diameter located along a generatrix of the body of revolution; the locations of the orifices are listed in Table 1.

The BLADEs are either one or two ribbon rings manufactured from 0.13-mm-thick ground spring steel and positioned equidistantly from the surface of the model. The leading and trailing edges of each ring are wedge shaped with a wedge angle of 40 deg. A fixed BLADE position in the boundary layer is ensured by using six radial cylindrical supports, 0.7 mm in diameter, whose angular separation

Table 1 Pressure orifice locations

Number	Location, mm	Number	Location, mm
1	109	12	900.3
2	150	13	950.1
3	194.3	14	1000.3
4	244.8	15	1100.5
5	294.5	16	1200.3
6	350.2	17	1400.3
7	420.3	18	1600.5
8	500.2	19	1800.3
9	650.4	20	2000.7
10	800.2	21	2200.5
11	850.1	22	2400.7

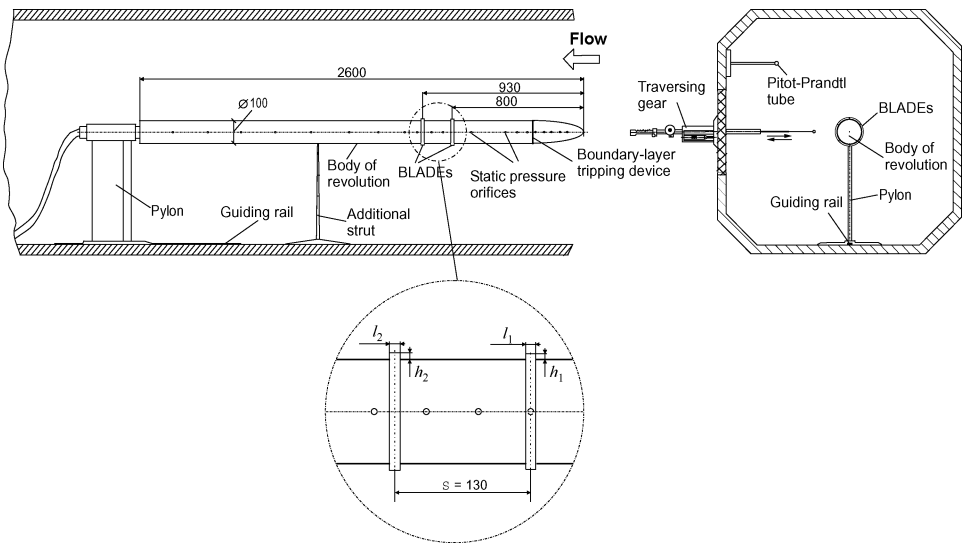

Fig. 1 Body of revolution schematic and BLADE geometric configuration, not to scale; all dimensions in millimeters.

Table 2 Major geometric characteristics of BLADEs

Configuration	l_1/δ_0	h_1/δ_0	$h_1 v_*/\nu$	l_2/δ_0	h_2/δ_0	$h_2 v_*/\nu$	s/δ_0	α, deg
1	0.77	0.31	274					0
2	0.77	0.44	384					0
3	0.77	0.60	527					0
4	0.77	0.76	673					0
5	0.77	0.87	765					0
6	0.77	1.03	914					0
7	0.77	0.44	381	0.85	0.50	431	10.6	0
8	1.02	0.43	380	1.11	0.49	410	10.4	0
9	1.37	0.43	380	1.48	0.49	413	10.4	0
10	0.77	0.44	381	0.85	0.50	431	10.6	1.8[a]

[a]For second BLADE element.

is 60 deg. The position of the supports across the boundary layer could be adjusted, and their diameter is chosen to minimize any possible support-induced drag. Several sets of BLADEs of various chord lengths, diameters, and angles of attack were manufactured. In all tests, the BLADEs are carefully aligned to be concentric with the axis of the body of revolution. The angles of attack relative to the model surface are controlled using a fine-line mask. The distances from the nose of the model to the midpoint of the upstream and downstream rings are 800 and 930 mm, respectively, in all experiments. The main geometric parameters of the BLADEs, normalized by the thickness δ_0 of the undisturbed boundary layer at the station where the first ring is installed, are given in Table 2. (The boundary-layer thickness δ_0 is taken to be at the location where $U/U_\infty = 0.99$.) The wall-normal position of each of ring within the boundary layer is also given in the law-of-the wall variables hv_*/ν. The tabulated data are presented for the experimental conditions with $Re_L = 4.35 \times 10^6$, which is the test condition for the most of the experiments.

Note also that the wall-normal position and chord length of the second ring (at the station $x = x_0 + s$) are selected to account for the boundary-layer thickening between the first and the second ring. That is, the characteristic parameters of the second ring when normalized with respect to the local boundary-layer thickness are approximately the same as those of the first ring.

The boundary-layer traverses are carried out by using a remotely controlled traverse gear having three degrees of freedom; the traverse gear is mounted on the sidewall of the wind-tunnel test section (Fig. 1). Because of limited length that could be traversed by the gear in the x direction, the model is designed to allow its displacement along the wind-tunnel test section using a guide rail. Precise positioning of the model relative to the freestream velocity vector is achieved by measurement of the total pressure P_0 from four geometrically identical Preston tubes installed at the wall of the body of revolution at the cross section $x = 2000$ mm in two diametrically opposite planes.

The dynamic pressure q_∞ in the freestream flow is determined from the difference between the total, P_0, and static, P_∞, pressure registered by a pitot–Prandtl tube, mounted at a distance of about five model diameters downstream of the body nose. The dynamic pressure is also determined from the difference $(P_{0s} - P_{ts})$ between the stagnation pressure in the settling chamber of the wind tunnel and the static pressure near the exit of the contraction.

The mean velocity U and the rms streamwise component of velocity fluctuations $\sqrt{u'^2}$ are measured using a DANTEC 55M single-component hot-wire constant temperature anemometer. The setup of the anemometer apparatus includes a 55M01 hot-wire bridge with a 55D10 linearizer connected to its output. The constant component of the linearized signal, corresponding to the mean flow velocity, is measured using a 55D31 digital dc voltmeter. The variable component of the signal, corresponding to the rms value of the streamwise velocity component $\sqrt{u'^2}$, is filtered by a 55D25 auxiliary unit and is measured by a 55D35 rms voltmeter. The fluctuating signal is visually observed using a C1–73 oscilloscope. As a primary measurement transducer, a miniature hot-wire probe with a single sensor made of tungsten wire with diameter of 5 μm and active length 1.2 mm long is used.

To determine local values of the skin-friction coefficient C_f, several methods are employed. In the cases where the flow velocity profile followed the law-of-the-wall (case with the initial model configuration), the well-known Preston tube method[19] was used. Depending on experimental conditions, two tubes with outside diameters of 1.06 and 1.61 mm and inner-to-outer diameter ratio of 0.62 are used. The skin-friction coefficient is calculated using the calibration method of Patel.[20] For manipulated boundary layers, we use the Clauser chart method, and in several cases, the momentum integral equation for a body with lateral curvature R:

$$\frac{\mathrm{d}\theta}{\mathrm{d}x} + \frac{\theta}{U_\infty}\frac{\mathrm{d}U_\infty}{\mathrm{d}x}(2+H) + \theta\left(\frac{1}{R}\frac{\mathrm{d}R}{\mathrm{d}x}\right) = \frac{\tau_w}{\rho U_\infty^2} \tag{1}$$

where θ is the momentum thickness, H is the shape factor of the boundary layer, and τ_w is the wall shear stress. The integral quantities in the momentum integral equation are determined from the measured boundary-layer profiles.

The random error in measuring the primary quantities of interest (the distance from the wall y, the streamwise coordinate x, the pressure coefficient C_p on the surface of the model, the dynamic pressure q_∞, the mean flow velocities U_∞ and U, the skin-friction coefficient C_f, and the rms value of velocity fluctuations $\sqrt{u'^2}$) are $y \pm 0.005$ mm, $x \pm 0.2$ mm, $C_p \pm 0.3\%$, $q_\infty \pm 0.25\%$, $U_\infty \pm 0.5\%$, C_f $3-5\%$, $U \pm 0.5\%$, and $\sqrt{u'^2} \pm 2\%$.

III. Results and Discussion

The goal of the present experiments was to examine the effectiveness of BLADE for drag reduction. Thus, it was necessary to first confirm the turbulent state of the boundary layer on the initial test configuration, that is, model without BLADE.

A. Characteristics of Regular Flow

Therefore, the initial stage of the study was an analysis of the state of the boundary layer on the initial model configuration. It was shown previously[17] that, starting from the distance $\bar{x} = x/L \geq 0.3$, on the body of revolution there is a stabilized flow region with uniform (within the experimental error) static pressure, $C_P = (P_i - P_\infty)/q_\infty \approx -0.007$. This means that a gradient-free flow is achieved over most of the model; this condition is maintained throughout the series of experiments.

To gain better insight into the regular boundary-layer flow, we examined in detail the profiles of mean flow velocity and streamwise velocity fluctuations, in the frequency band of 1–50,000 Hz, and the skin-friction measurements at 14–15 stations over the length of the model. The ratio of the boundary-layer thickness on the body of revolution to the cross-sectional radius of the body varied in the range 0.27–0.52, that is, this ratio is such that the analysis of characteristics of the shear flow could not made using the traditional approach that is applied to flat boundary layers. Therefore, our analysis takes into account the effect of lateral curvature.[21] Figure 2 presents semilogarithmic plots of experimental profiles of flow velocity in the law-of-the-wall variables $U^+ = f(\log \eta^+)$,

$$U^+ = \frac{U}{v_*}, \qquad \eta^+ = \frac{4\eta}{\left(1 + \sqrt{1 + \eta/\eta_0}\right)^2}$$

where $\eta = y v_*/\nu$ and $\eta_0 = R v_*/\nu$ are the nondimensional coordinates normal to the wall and $v_* = \sqrt{(\tau_w/\rho)}$ is the dynamic velocity. For comparison, Fig. 2 also shows the canonical velocity profile $U^+ = A \log y^+ + B$, with the values $A = 5.62$ and $B = 5.0$, as recommended in Ref. 22. It is seen that for all values of $\bar{x}$ the profiles are as expected and correlate well with the canonical profile. This allows us to conclude that, to a first approximation, a developed boundary layer is established downstream of the second measuring station.

Figure 3 shows the streamwise variation of the momentum thickness,

$$\theta = \int_0^\delta \frac{U}{U_e}\left(1 - \frac{U}{U_e}\right)\left(1 + \frac{y}{R}\right)\mathrm{d}y \tag{2}$$

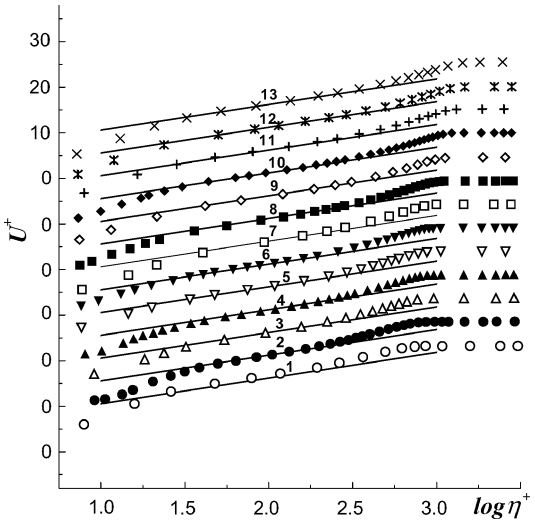

Fig. 2 Streamwise mean velocity profiles in law-of-the-wall variables for regular boundary layer at $Re_L = 4.35 \times 10^6$; $x/L =$ 1, 0.252; 2, 0.308; 3, 0.327; 4, 0.346; 5, 0.365; 6, 0.385; 7, 0.423; 8, 0.461; 9, 0.538; 10, 0.615; 11, 0.692; 12, 0.769; and 13, 0.846: ——, $U^+ = 5.62 \log y^+ + 5$, following Ref. 22.

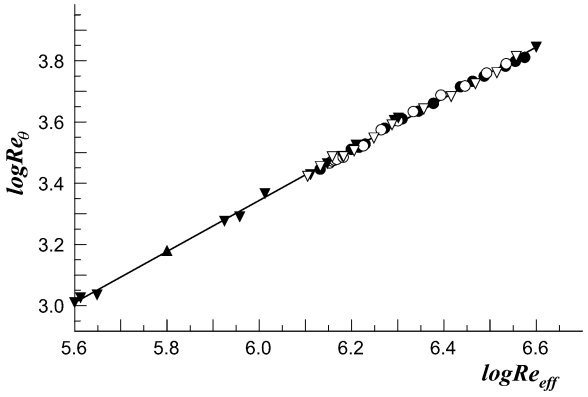

Fig. 3 Different test runs, $\log Re_\theta$ vs $\log Re_{\text{eff}}$ for regular boundary layer.

a quantity that is analogous to the flat-plate momentum thickness; the data are obtained in different series of tests and are presented here in the form $\log Re_\theta = f(\log Re_{\text{eff}})$, where Re_{eff} is the Reynolds number based on the coordinate x_{eff}. (Here x_{eff} is the coordinate that characterizes the virtual origin of the turbulent boundary layer. It is defined from the condition of equality at the first measuring station between the experimental value of θ and its value obtained from the Spalding procedure[23] and from a subsequent calculation in the upstream direction to the point x where the momentum thickness is zero.) It is seen that over the range of Reynolds numbers that are examined there is a linear dependence, which is indicative of the formation of a developed turbulent flow even at the lower values of Reynolds number Re_{eff}.

The distributions of all other integral characteristics also show the expected features. Nonetheless, there arises the question as to what extent these distributions are similar to the analogous distributions on a body with the same lateral curvature. In this regard, Fig. 4 shows a comparison, in the form $C_f = f(\log Re_{\text{eff}})$, of the experimental and predicted values of the local skin-friction coefficient C_f. It is seen that the data determined using the method in Ref. 24, which requires no empirical data except for the radius of curvature of the body, agree within approximately 5% of the experimental values of C_f. On the other hand, the measured results derived from the velocity profiles (according to the Clauser method) show generally good agreement with the Preston tube results to within approximately 3% (Ref. 17).

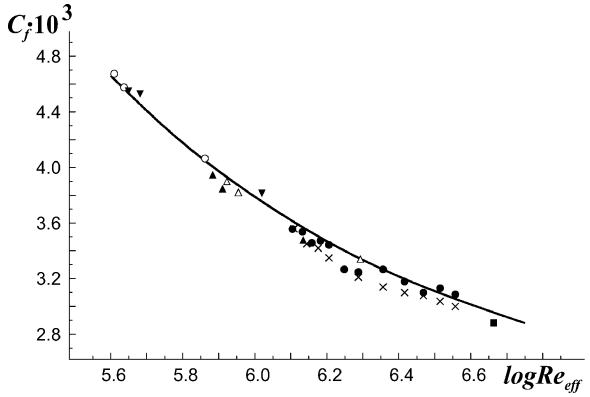

Fig. 4 Variation of local skin-friction coefficient with $\log Re_{\text{eff}}$ for regular boundary layer: symbols, experiment, $Re_L = (1.44 - 5.54) \times 10^6$ and ——, calculation according to Ref. 24.

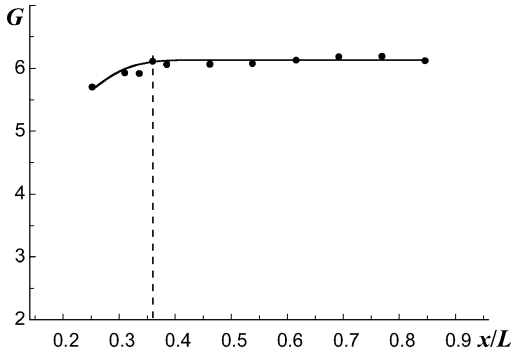

Fig. 5 Nonequilibrium Clauser parameter for regular boundary layer at $Re_L = 4.35 \times 10^6$; – – –, location of second ring element for manipulated boundary layer.

The nonequilibrium Clauser parameter

$$G = \sqrt{2/C_f}[(H-1)/H] \tag{3}$$

is roughly uniform along the coordinate $\bar{x} = x/L$ (Fig. 5). This is indicative of the formation of an equilibrium turbulent boundary layer from at least the station where the BLADE is installed (as shown by the dashed line). Note, however, that the observed value of G is approximately 13% smaller than on a flat plate under similar conditions, where it has a value of 6.7 (Ref. 25).

Other experimental results, including the distribution of turbulent velocity fluctuations, confirm that the characteristics of the flow on the body of revolution without BLADE are quite consistent with that of a turbulent boundary layer that develops in nominally gradient-free flow over a body with lateral curvature.

B. Characteristics of Manipulated Flow

With BLADEs installed in the boundary layer, the pressure distribution displays no extra-ordinary features except in the close vicinity of the device. In this region where the BLADE is deployed, the pressure coefficient C_p decreases, presumably due to flow acceleration in the region between the ribbon ring and the surface of the body. In addition, there is a short region of increased pressure immediately in front of the BLADE. On the whole, although the magnitude of C_p goes beyond the experimental error at several points over the length of the model, over the most of the body the distribution of pressure is quite regular, and the pressure data agree with the data in the regular flow.

As an example, Fig. 6 shows the boundary-layer velocity profiles $U/U_e = f(y)$ of the tandem configuration BLADE 8 for various nondimensional distances $\Delta x/\delta_0$ measured downstream of the trailing edge of the second ring element. It is seen that a distinct narrow wake exhibiting a velocity defect at the BLADE height (shown by the horizontal dashed–dotted line) forms in the region downstream

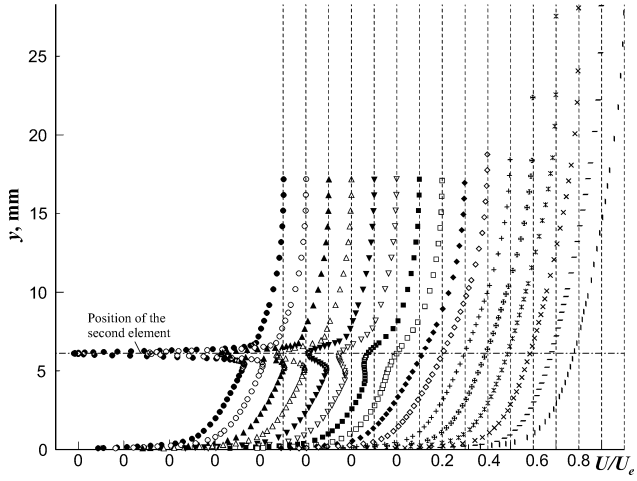

Fig. 6 Boundary-layer streamwise mean velocity profiles behind BLADE 8 at $Re_L = 4.35 \times 10^6$; values of $\Delta x/\delta_0$: ●, 0.059; ○, 0.230; ▲, 0.452; △, 0.748; ▼, 0.970; ▽, 1.711; ■, 2.452; □, 4.674; ◆, 12.081; ◇, 19.489; +, 26.896; ✠, 34.304; ∗, 49.119; ×, 63.933; -, 78.748; and |, 93.563.

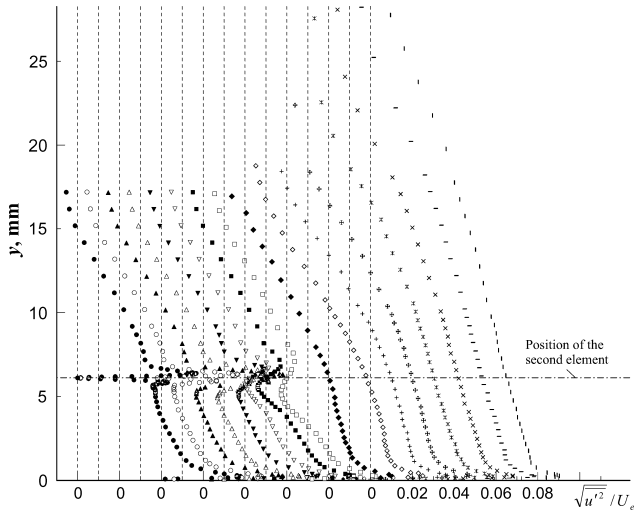

Fig. 7 Boundary-layer rms streamwise velocity fluctuation profiles behind BLADE 8; symbols same as in Fig. 6.

of the BLADE; this wake smoothly dissipates in the downstream direction. The rate of smearing of the velocity defect along the streamwise coordinate decreases with increasing height of the BLADE in the boundary layer.[17] This observation provides additional indirect evidence that there is a longer memory in the outer part of the boundary layer in relation to the flow disturbances.

A similar effect is seen in the profiles of streamwise velocity fluctuations $\sqrt{\overline{u'^2}}/U_e = f(y)$ (Fig. 7); the only difference is that the characteristic deformation of the profile of $\sqrt{\overline{u'^2}}$ persists to a more downstream distance. Nevertheless, a pronounced suppression of velocity fluctuations is observed downstream of the BLADE (Fig. 8) in the region between the wall and the height of the BLADE. Note also that, in the flow region above the BLADE, no substantial increase of the turbulent fluctuations is observed. This observation is consistent with the previously reported mechanism,[3] namely, that a thin ribbon hampers the momentum exchange between the outer and inner layers of the boundary layer, thus resulting in a delay of the growth of the momentum thickness over the length of the model and, therefore, promoting turbulent skin-friction reduction.

Note also that the difference between the profiles of $\sqrt{\overline{u'^2}}$ in the presence of the BLADE and the initial configuration decreases in the downstream direction. Nonetheless, the "suppressing" action of such ring manipulators, in the tandem configuration, is observed up to a distance of $62\delta_0$.

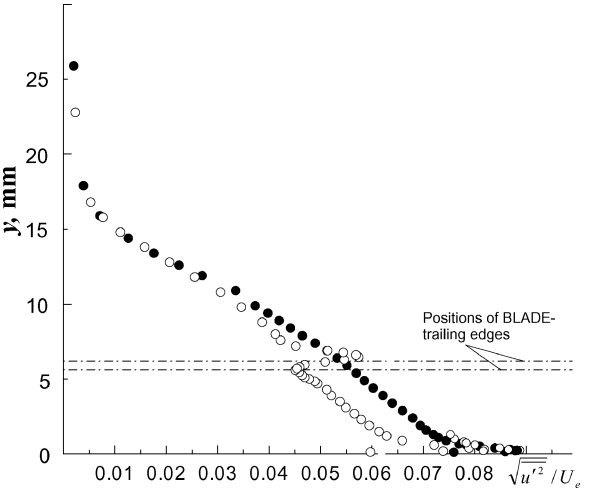

Fig. 8 Comparison of streamwise velocity fluctuation profiles for regular and manipulated boundary layer at $\Delta x/\delta_0 = 1.07$ and $Re_L = 4.35 \times 10^6$: ●, no BLADEs and ○, BLADE 7.

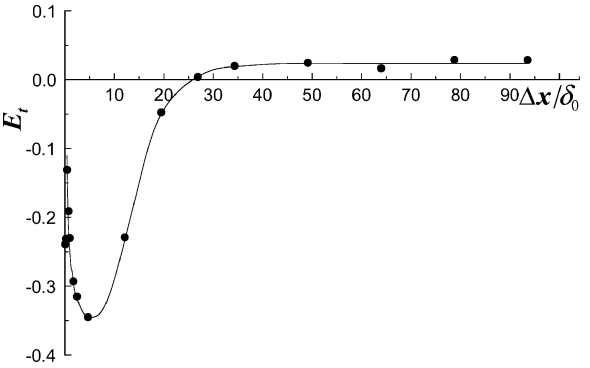

Fig. 9 Variation of excess kinetic energy downstream of BLADE 8, $Re_L = 4.35 \times 10^6$.

It is also of interest to evaluate the integral effect due to the change in turbulent velocity fluctuations, including the region over the BLADE. This evaluation is made in terms of the nondimensionalized thickness of the excess kinetic energy for the fluctuating velocity u'^2:

$$E_t = \frac{\int_0^1 \left(\overline{u'^2_{\text{blade}}} - \overline{u'^2}\right) \mathrm{d}(y/\delta)}{\int_0^1 \left(\overline{u'^2}\right) \mathrm{d}(y/\delta)} \tag{4}$$

where u'^2_{blade} and u'^2 are the fluctuating velocity in the manipulated and regular boundary layer, respectively and the overbar denotes a time mean value. The results are presented in Fig. 9 for the BLADE 8 configuration and the streamwise distribution $E_t = f(\Delta x/\delta_0)$ is shown. Here, the value $E_t = 0$ (abscissa axis) refers to the initial state (regular flow), and the deviation from $E_t = 0$ can be interpreted as either an increase or a decrease of integral turbulent velocity fluctuations downstream of BLADE due to the manipulation of the flow.

It can be seen that there is a distinct decrease in E_t up to a distance of $\Delta x = 25\delta_0$ downstream of the BLADE. Farther downstream, $\Delta x \geq 25\delta_0$, the value of E_t increases somewhat in excess of the corresponding value for the regular flow. At present it has not yet been clearly determined whether this difference is within the experimental error or indeed there is an opposite effect in this flow region. In any case, the uniformity of the experimental data shows no anomalous distribution of $E_t = f(\Delta x/\delta_0)$ in this region.

The distributions of the displacement thickness δ^*, the momentum thickness θ, and the boundary-layer shape factor H for all BLADE configurations show features that are different from the regular flow only in a short region behind the BLADE. For example,

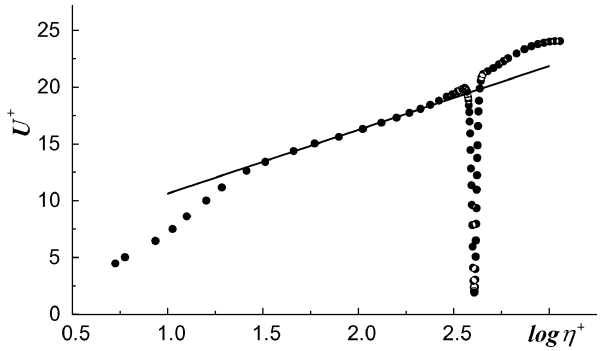

Fig. 10 Streamwise mean velocity profile in the law-of-the-wall variables at $\Delta x/\delta_0 = 1.07$, BLADE 2: ——, $U^+ = 5.62 \log y^+ + 5$, according to Ref. 22.

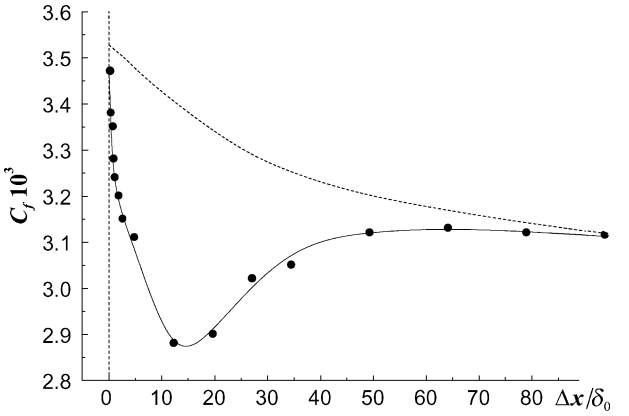

Fig. 11 Local skin-friction distribution downstream of BLADE 8 at $Re_L = 4.35 \times 10^6$: - - - -, regular boundary layer (averaged data).

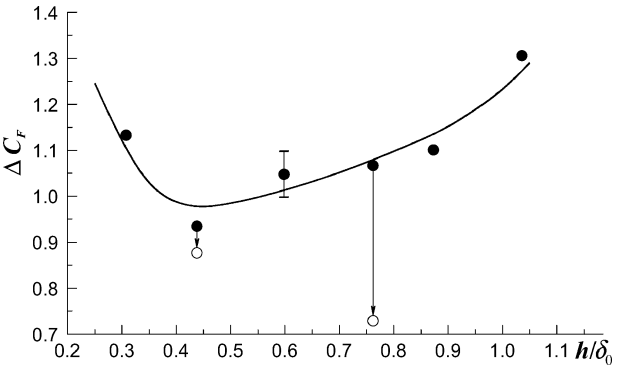

Fig. 12 Effect of wall-normal position on drag reduction for a single-element BLADE (configurations 1–6) of fixed chord length $l/\delta_0 = 0.77$; $Re_L = 4.35 \times 10^6$ and $\Delta x/\delta_0 = 62.6$: ○, tandem configurations with and without angle of attack.

in the tandem BLADE configuration, the value of θ increases by approximately 5% at the first measurement station, $\Delta x = 0.5$ mm. Apparently, this increase is caused by the BLADE-induced drag. However, the rate of increase of θ in the downstream direction is lower than on the initial configuration; this is, of course, the factor that provides for the observed skin-friction reduction. Although the curve $\theta = f(\Delta x/\delta_0)$ for single-element BLADEs shows a similar behavior, the difference from the initial configuration is less pronounced.

One of the main indications of effectiveness of BLADE is the local skin-friction coefficient. It was shown in Ref. 17 that most methods (especially empirical methods) are not very reliable in estimating the effectiveness of the BLADE for flows with appreciable (over the length of the model) gradients of C_f downstream of BLADE. Direct measurement of the local skin friction is very sensitive to the drag balancing instrument, whereas the other common methods of indirect determination of C_f are subject to other types of errors. It is, therefore, necessary to measure the drag with a sensitive enough instrument. The preferred methods are the Preston method and the Clauser chart method, which normally yield similar results. Note, however, that one can use the Clauser chart method to analyze skin friction at BLADE heights h below some minimum value. As an example, Fig. 10 shows the experimental profile of flow velocity directly behind the BLADE trailing edge in the law-of-the-wall variables. It is seen that there is a distinct narrow wake ($\log \eta^+ \approx 2.6$) with a velocity defect at the BLADE height. However, this wake has almost no effect on the logarithmic region of the boundary layer. Indeed, except for the narrow wake region, the profile closely follows the classical profile (shown by the solid line). This validates the use of the Clauser chart method, which is known to be applicable if the law-of-the-wall holds in the boundary layer. In support of this, the results of Bertelrud at al.,[10] where the values C_f are obtained by Preston method, can be considered. With these C_f known, the experimental velocity profiles are presented in this paper in law-of-the-wall coordinates. As seen from these results, from $\Delta x/l = 0.1$ downstream, the profiles rapidly become similar. For our test cases, the value $\Delta x/l = 0.1$ corresponds to the value $\Delta x/\delta_0 \approx 0.07$–$0.13$ depending the BLADE length. This means that the streamwise region without similarity is less than $\Delta x/\delta_0 \approx 0.13$.

The data obtained using the Clauser chart method are reported in Ref. 17 for a single-element BLADE whose position h is varied over the height of the boundary layer. In all cases, the value of C_f decreases sharply immediately downstream of the BLADE; the location of the minimum C_f shifts in the downstream direction with increasing h. In this respect, the distribution of C_f is similar to the case of a flat plate.[11,15] As regards a tandem arrangement, in most previous studies of two-dimensional, flat-plate, boundary layers, the use of this arrangement usually leads to further improvement in drag reduction (for example, Ref. 10). Figure 11 shows experimental skin-friction coefficient data for the tandem configuration BLADE 8. For comparison, here we also show averaged data obtained on the initial configuration (dotted line). As in the earlier cases, here the value of C_f at $\Delta x/\delta_0 \leq 15$ is much smaller than in the regular boundary layer. With increasing $\Delta x/\delta_0$, C_f first sharply decreases and, then, gradually, approaches that in the regular boundary layer. Clearly, in this region there is an energy exchange from the external flow to the inner part of the boundary layer, which results in fuller velocity profiles and, hence, in increased skin friction. With this BLADE, the maximum reduction in turbulent skin friction is about 16%.

Of interest is an estimate of the effectiveness of the BLADEs in terms of net drag reduction. This quantity is known to be the sum of two components, the first being the skin-friction reduction due to BLADE and the second the device-induced drag. It is common practice to characterize the effectiveness of the BLADE in terms of the drag reduction ratio ΔC_F (Refs. 3, 10, and 11):

$$\Delta C_F(x) = \frac{\left[Re^{**}(x) - Re^{**}(x_0)\right]_{\text{blade}}}{Re^{**}(x) - Re^{**}(x_0)} \tag{5}$$

This measure of the drag reduction includes the BLADE-induced losses. Here Re^{**}_{blade} and Re^{**}_0 are the Reynolds numbers based on the momentum thickness at stations x and x_0 for the model with BLADE (in the numerator) and for the initial configuration (in the denominator). A ΔC_F of less than unity indicates a net drag reduction, whereas a ΔC_F greater than unity indicates a net drag increase.

It is seen that, although the magnitude of ΔC_F decreases with distance from the BLADE trailing edge, most of the single-element BLADEs do not yield a beneficial net drag reduction (Fig. 12). As can be seen, the minimum of ΔC_F is attained for $h/\delta_0 = 0.45$. This observation casts doubt on the practicability of positioning the BLADE near the outer edge of the boundary layer, as would be suggested from the results of flat-plate experiments.

The results of the tandem configurations are shown in Fig. 13. In this configuration, from $\Delta x \approx 15\delta_0$ downstream to 90–$100\delta_0$, a reduction in the net drag is observed. This reduction is as much

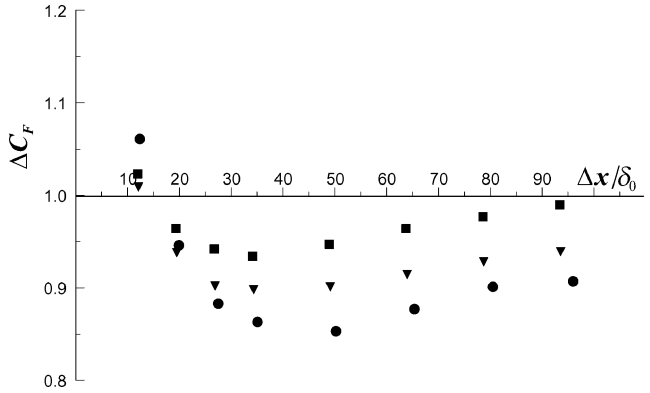

Fig. 13 Effect of chord length on drag reduction of tandem BLADE configuration at $Re_L = 4.35 \times 10^6$; values of device chord length: ●, $l_1/\delta_0 = 0.77$ and $l_2/\delta_0 = 0.85$; ▼, $l_1/\delta_0 = 1.02$ and $l_2/\delta_0 = 1.11$; and ■, $l_1/\delta_0 = 1.37$ and $l_2/\delta_0 = 1.48$ (BLADE configurations 7–9).

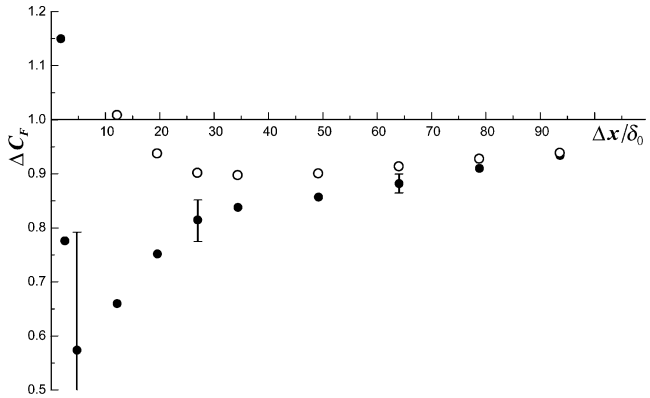

Fig. 14 Drag reduction for ●, tandem BLADE 10 ($\alpha = 1.8$ deg) compared to ○, tandem BLADE 7 ($\alpha = 0$ deg); $Re_L = 4.35 \times 10^6$.

as 15% at $\Delta x/\delta_0 \approx 50$. The minimum in ΔC_F is caused by the reduction of the skin-friction component, which is a minimum at this point. Also note the marked effect of the BLADE chord length l. An increase in l makes the net drag reduction less pronounced. An explanation of this may be given as follows. Because, with all other conditions constant, the contribution due to pressure forces also remains approximately constant as l is varied, it is evident that the less pronounced net drag reduction is caused by an increase in the parasitic device drag. Note, however, that, generally speaking, this behavior of ΔC_F with respect to the chord of the BLADE is different from results of flat-plate experiments.[11] The reasons for the observed difference still remain unclear. Most probably, the underlying causes are related to specific features of the flow around a body with appreciable lateral curvature.

The results of the experiments suggest that the effectiveness of the tandem BLADE configuration maybe increased by installing the BLADE at a small positive angle of attack ($\alpha = 1.8$ deg). In Fig. 14, the ΔC_F distribution for tandem configuration BLADE 10 at $\alpha = 1.8$ deg and its counterpart BLADE 7 ($\alpha = 0$ deg) are shown together. Both distributions indicate an initial sharp decrease in ΔC_F at small $\Delta x/\delta_0$, culminating with a maximum reduction of 10% at (35–45)δ_0 for BLADE 7 and a corresponding reduction of 40% at (5–8)δ_0 for BLADE 10. Thus, it can be seen that the effect is quite considerable. At larger $\Delta x/\delta_0$, ΔC_F for both distributions increase monotonically to the no-BLADE configuration ($\Delta C_F = 1$). Note that the random measurement error in ΔC_F is significantly larger at smaller $\Delta x/\delta_0$. This increased error arises because the random error in the determination of value θ is ± 0.025 mm; therefore, the contribution of this error into integral increases with decreasing $\Delta x/\delta_0$. Nevertheless, there is a smooth distribution of ΔC_F that suggests that the results are reliable. Also note that the effect of the small positive angle of attack is quite pronounced when the BLADE is placed at $h/\delta_0 = 0.75$ (Fig. 12, vertical arrow).

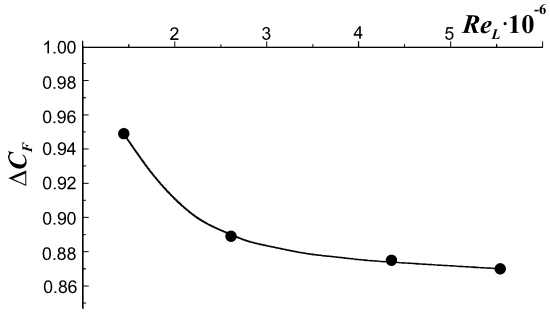

Fig. 15 Effect of Reynolds number on drag reduction for tandem BLADE 7 at $\Delta x/\delta_0 = 65.3$.

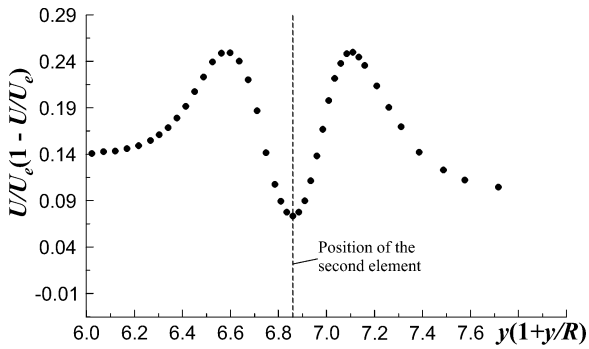

Fig. 16 Distribution of subintegral function for BLADE 8 at $\Delta x/\delta_0 = 1.07$.

It is also of interest to examine the Reynolds number effect on the effectiveness of the tandem BLADE configuration. The tandem configuration BLADE 7 (Fig. 15) shows the dependence $\Delta C_F = f(Re_L)$ observed at $\Delta x/\delta_0 = 65.3$. (Here, the Reynolds number was varied by changing the freestream velocity; the characteristic length in the Reynolds number is the length L of the model.) Although the range of Reynolds numbers Re_L is not very large, the observed behavior of the curve suggests that, with increasing Reynolds number, the effectiveness of the BLADEs does not decrease. On the other hand, the highest-Reynolds-number data of our work are close to the minimum-Reynolds-number data of the Anders paper,[26] where the dependence of drag reduction on Reynolds number was documented from a test on an axisymmetric body in a tow tank. At higher Reynolds numbers, the skin-friction reduction in the Anders data is small. This means that the expectation of drag reduction on a full-scale vehicle is uncertain.

Finally we clarify the mechanism that is responsible for skin-friction reduction in the manipulated boundary layer. The skin-friction reduction [Eq. (5)] is dependent on the subintegral function $U/U_e(1 - U/U_e)$ that appears in the expression for θ, Eq. (2). The presence of two symmetrically located maxima in the subintegral function measured behind the BLADE (Fig. 16) and the discrete tone observed in the frequency spectra of velocity fluctuations indicate that there is a vortex street in the wake of the BLADE. For the present experiments, the Reynolds numbers Re_t based on the local freestream velocity and the thickness t of the ribbon ring are in the range from 174 to 206, which is within the range whereby the formation of a von Kármán street is possible. Because the von Kármán vortex street has a well-ordered structure, the presence of this flow feature may be a necessary condition for turbulent skin-friction reduction (see Ref. 10). Specifically, the eddies in the wake of the BLADE interact with the turbulence in the ambient flow to change the characteristic scale of high-energy vortices. This change promotes the redistribution of the turbulence energy, which results in the skin-friction reduction. The data presented in Ref. 18 show that, with increasing wall-normal distance of BLADE, the "intensity" of the vortex street is significantly weakened. This observation suggests that it is not prudent to position BLADEs near the outer edge of the boundary layer, at least in the case of bodies of revolution.

IV. Conclusions

An experimental study of the effectiveness of BLADEs installed in the developed incompressible turbulent boundary layer formed on an axisymmetric body of revolution in nominally gradient-free flow was conducted. The measurements lead to the following conclusions:

1) All BLADE configurations, including single-element ones, show a reduction in skin-friction. The maximum reduction is 7.5–16%, and this magnitude depends on the wall-normal position of the BLADE. Most of the single-element BLADEs do not result in a net drag reduction compared with regular boundary layers. An exception is the single-element BLADE that is positioned at a distance of $0.45\delta_0$ from the wall. This is different from the results that are obtained in a two-dimensional, flat-plate, boundary layer, where the optimum is observed at a height of $0.75\delta_0$.

2) The tandem BLADE configuration provides an effective means for altering the near-wall turbulence and, therefore, results in a net drag reduction. From $\Delta x \approx 15\delta_0$ downstream of the trailing edge of the second ring element and up to $90–100\delta_0$, a significant net drag is observed. The maximum reduction of 15% occurs at $\Delta x/\delta_0 \approx 50$. The effectiveness of the BLADEs decreases appreciably with increasing relative BLADE length and increases when the BLADE has a small positive angle of attack, $\alpha = 1.8$ deg.

3) The effectiveness of the BLADEs does not decrease with increasing Reynolds number. However, the results of the Anders paper, where the dependence of drag reduction on Reynolds number was documented from a test on an axisymmetric body in a tow tank, show that the skin-friction reduction is strongly reduced at higher Reynolds numbers. This means that the expectation of drag reduction on a full-scale vehicle is uncertain.

References

[1]Bushnell, D. M., "Turbulent Drag Reduction of External Flows," AIAA Paper 83-0227, Jan. 1983.

[2]Hefner, J. N., "Drag Reduction Problem," *Aerospace America*, Vol. 26, No. 1, 1988, pp. 14–16, 19, 20, 22, 24, 26, 27.

[3]Bushnell, D. M., and Hefner, J. N. (eds.), *Viscous Drag Reduction in Boundary Layers*, Vol. 123, Progress in Astronautics and Aeronautics, AIAA, Washington, DC, 1990, pp. 3–50.

[4]Coustols, E., and Savill, A. M., "Turbulent Skin-Friction Drag Reduction by Active and Passive Means," Pt. 1–2; reprinted from AGARD Rept. 786, 1992, pp. 8-1–8-80.

[5]Choi, K.-S., "European Drag-Reduction Research—Recent Developments and Current Status," *Fluid Dynamic Research*, Vol. 26, No. 5, 2000, pp. 325–335.

[6]Lofdahl, L., and Gad-el-Hak, M., "MEMS Applications in Turbulence and Flow Control," *Progress in Aerospace Sciences*, Vol. 35, 1999, pp. 101–203.

[7]Wark, C. E., Naguib, A. M., and Nagib, H. M., "Effect of Plate Manipulators on Coherent Structures in a Turbulent Boundary Layer," *AIAA Journal*, Vol. 28, No. 11, 1990, pp. 1877–1884.

[8]Guezennec, Y. G., and Nagib, H. M., "Mechanisms Leading to Net Drag Reduction in Manipulated Turbulent Boundary Layers," *AIAA Journal*, Vol. 28, No. 2, 1990, pp. 245–252.

[9]Sahlin, A., Alfredsson, P. H., and Johansson, A. V., "Direct Drag Measurement for a Flat Plate with Passive Boundary Layer Manipulators," *Physics of Fluids*, Vol. 29, No. 3, 1986, pp. 696–700.

[10]Bertelrud, A., Truong, T. V., and Avellan, F., "Drag Reduction in Turbulent Boundary Layers Using Ribbons," AIAA Paper 82-1370, Aug. 1982.

[11]Plesniak, M. W., and Nagib, H. M., "Net Drag Reduction in Turbulent Boundary Layers Resulting from Optimized Manipulation," AIAA Paper 85-0518, March 1985.

[12]Gudilin, I. V., Enyutin G. V., Kim, A. Y., Lashkov, Y. A., and Shumilkin, V. G., "Experimental Study of Combined Effect of Riblets and Eddy Breakup Devices on Turbulent Skin Friction," *Uchenye Zapiski TSAGI*, Vol. 20, No. 6, 1989, pp. 8–14 (in Russian).

[13]Gudilin, I. V., Lashkov, Y. A., and Shumilkin, V. G., "Combined Effect of Riblets and Eddy Breakup Devices on Flat-Plate Turbulent Skin Friction," *Izvestiya Akademii Nauk, Mekhanika Zhidkosti i Gaza*, No. 3, May–June 1995, pp. 39–46 (in Russian).

[14]Kuzenkov, V. K., Levitskii, V. N., Repik, E. U., and Sosedko, Y. P., "Investigation into the Mechanism of Turbulent Skin-Friction Reduction with the Help of Eddy Breakup Devices," *Izvestiya Akademii Nauk, Mekhanika Zhidkosti i Gaza*, No. 5, Sept.–Oct. 1996, pp. 80–89 (in Russian).

[15]Savill, A. M., and Mumford, J. C., "Manipulation of Turbulent Boundary Layers by Outer-Layer Devices: Skin-Friction and Flow-Visualization Results," *Journal of Fluid Mechanics*, Vol. 191, 1988, pp. 389–418.

[16]Gudilin, I. V., Lashkov, Y. A., and Shumilkin, V. G., "Experimental Study of the Effect of Riblets and Eddy Breakup Devices on the Drag of a Body of Revolution," *Izvestiya Akademii Nauk, Mekhanika Zhidkosti i Gaza*, No. 3, May–June 1996, pp. 154–157 (in Russian).

[17]Gorshkov, V. G., and Kornilov, V. I., "Influence of Eddy Breakup Devices on Characteristics of Turbulent Boundary Layer on a Body of Revolution," Inst. of Theoretical and Applied Mechanics, Preprint 4-2003, Russian Academy of Science, Siberian Branch, Novosibirsk, Russia, 2003, pp. 1–43 (in Russian).

[18]Gorshkov, V. G., and Kornilov, V. I., "Turbulent Boundary Layer on a Body of Revolution Under Influence of Eddy Breakup Devices," *Proceedings of International Conference on the Methods of Aerophysical Research*, Pt. 1, Nonparel, Novosibirsk, Russia, 2004, pp. 112–117.

[19]Preston, J. H., "The Determination of Turbulent Skin Friction by Means of Pitot Tubes," *Journal of the Royal Aeronautical Society*, Vol. 58, March 1954, pp. 109–121.

[20]Patel, V., "Calibration of the Preston-Tube and Limitations on Its Use in Pressure Gradient," *Journal of Fluid Mechanics*, Vol. 23, Pt. 2, 1965, pp. 185–208.

[21]Smits, A. J., and Joubert, P. N., "Turbulent Boundary Layers on Bodies of Revolution," *Journal of Ship Research*, Vol. 26, No. 2, 1982, pp. 135–147.

[22]"Computation of Turbulent Boundary Layers—1968," *Proceeding of AFOSR–IFP–Stanford Conference*, Vol. 2, edited by D. E. Coles and E. A. Hirst, Thermosciences Div., Dept. of Mechanical Engineering, Stanford Univ., Stanford, CA, 1969.

[23]Spalding, D. B., "A New Analytical Expression for the Drag of a Flat Plate Valid for Both the Turbulent and Laminar Regimes," *International Journal of Heat and Mass Transfer*, Vol. 5, Dec. 1962, pp. 1133–1138.

[24]Kovalenko, V. M., and Shulemovich, V. M., "Turbulent Boundary Layer on Circular Cylinder," *Izvestiya Akademii. Nauk, Seriya Tekhnicheskikh Nauk*, Vol. 13, No. 3, 1972, pp. 8–16 (in Russian).

[25]Kornilov, V. I., and Mekler, D. K., "Investigation into Boundary-Layer Memory to 2D Disturbances," Inst. of Theoretical and Applied Mechanics, Preprint 32-87, USSR Academy of Sciences, Siberian Branch, Novosibirsk, Russia, 1987, pp. 1–45 (in Russian).

[26]Anders, J. B., "LEBU Drag Reduction in High Reynolds Number Boundary Layers," AIAA Paper 89-1011, March 1989.

N. Chokani
Associate Editor